NJC

Accepted Manuscript

This is an *Accepted Manuscript*, which has been through the Royal Society of Chemistry peer review process and has been accepted for publication.

Accepted Manuscripts are published online shortly after acceptance, before technical editing, formatting and proof reading. Using this free service, authors can make their results available to the community, in citable form, before we publish the edited article. We will replace this *Accepted Manuscript* with the edited and formatted *Advance Article* as soon as it is available.

You can find more information about *Accepted Manuscripts* in the Information for Authors.

Please note that technical editing may introduce minor changes to the text and/or graphics, which may alter content. The journal's standard Terms & Conditions and the Ethical guidelines still apply. In no event shall the Royal Society of Chemistry be held responsible for any errors or omissions in this *Accepted Manuscript* or any consequences arising from the use of any information it contains.

ROYAL SOCIETY OF CHEMISTRY

www.rsc.org/njc

Journal Name

ARTICLE

Fe_3O_4 nanoparticles anchored layered graphene film for high performance lithium storage

Received 00th January 20xx,
Accepted 00th January 20xx

DOI: 10.1039/x0xx00000x

www.rsc.org/

Yu Liu,[a] * Yinqiao Zhan[b] Yulong Ying[b] and Xinsheng Peng[b]

Flexible and binder-free Fe_3O_4/graphene film was prepared through vacuum filtration of Fe_3O_4/GO suspensions, followed by an annealing process. Cross-sectional SEM images of the sandwiched films show that Fe_3O_4 nanoparticles homogeneously decorated onto layered graphene nanosheets and formed a nanoporous networks structure. Thus, the composite film provided effective channels to promote electrolyte penetration when used as anode for Li-ion batteries. Moreover, the good connection between Fe_3O_4 and graphene derived from hydrogen bonding or intermolecular force making them beneficial to charge transfer. The unique film with excellent mechanical stability also can buffer the volume expansion during Li-ion insertion/extraction process. After electrochemical tests, the as-prepared binder-free Fe_3O_4/graphene hybrid lamellar films demonstrated excellent cyclic retention with the specific capacity of 681.2 mA h g^{-1} after 50 cycles, which is 3 times higher than the discharge capacity of 222.0 mA h g^{-1} for pure Fe_3O_4, as well as good rate capability, making it promising candidates for use as Li-ion batteries anodes.

1. Introduction

Li-ion batteries (LIBs) with high capacity, long lifetime, high energy and large power density, have become the dominant power sources in portable electronic devices.[1,2] For now, the commercial graphite anode materials cannot satisfy the ever-increasing and urgent demands of high-power applications for its low theoretical capacity. Therefore, different transition metal oxides such as CuO, TiO_2, SnO_2 and Fe_3O_4 usually show much higher theoretical capacity (650-950 mA h g^{-1}) than graphite (only 372 mA h g^{-1}) are effective alternatives for next generation LIBs.[3-6] Among them, Fe_3O_4 is even promising in virtue of its high theoretical capacity (926 mA h g^{-1}), good electronic conductivity, natural abundance, non-toxic and low cost.[7,8] However, when used in practical application, Fe_3O_4 anodes usually suffer severe capacity degradation, resulting from both the quick aggregation of nanoparticles during cycling and large volume change (ca. 200%) during lithiation/delithiation process.[6,9-11]

Recent research shows that carbon (amorphous carbon and graphene) coating can effectively prevent electrochemical aggregation and accommodate the large volume change.[9,10,12] For example, Hu's group developed a magnetic field-induced solvothermal method to synthesize Fe_3O_4/C composite microrods. The as-prepared composite microrods exhibit significantly enhanced reversible capacity of ~650 mA h g^{-1} retained after 100 cycles.[13] Gao and coworkers prepared Fe_3O_4@C/CNT grapecluster structures show a much improved performance (a reversible capacity exceeding 900 mA h g^{-1}) compared with the Fe_3O_4@C composites.[14] Wang et al. synthesized flexible free-standing hollow Fe_3O_4/graphene films through vacuum filtration and thermal reduction processes. The composites exhibited a high specific capacity.[15] Other different structures of Fe_3O_4/graphene composites were also reported for the improved electrochemical performance.[16-18]

Many reports predict that flexible energy store device will be widely used in conventional electronics and some new devices such as wearable devices and implanted medical devices.[19,20] Graphene paper, due to its good electronic transport property and mechanical flexibility, has potential in flexible and bendable energy storage application.[15,21,22] However, aggregation between graphene nanosheets usually lead to severely reduced effective specific surface area and capacity when used as anodes in LIBs.[3] In this study, we develop a facile and green method with the aid of hydrogen bonding or intermolecular force in aqueous solution, as well as the following filtration and annealing process to prepare free-standing Fe_3O_4/graphene composite films. The thickness, quality and composition ratio of the films can be easily controlled during the preparation process. In the unique structure, Fe_3O_4 nanoparticles decorated onto stratified graphene nanosheets not simply intercalated into graphene nanosheets, the good connection is advantage for fast electron transfer between the Fe_3O_4 nanoparticles and graphene, resulting in enhanced electrochemical properties. When directly used as binder-free anode, the sandwich-type film can effectively prevent the aggregation of both graphene nanosheets and Fe_3O_4 nanoparticles, facilitating the electron transfer and the diffusion of Li^+ ions inside the films. More importantly, graphene can accommodate the volume change of Fe_3O_4 nanoparticles in charge-discharge process. Thus, the as-prepared Fe_3O_4/graphene achieve a stable reversible capacity up to 681.2 mA h g^{-1} after 50 cycles, much higher than 222.0 mA h g^{-1} of pure Fe_3O_4 nanoparticles.

[a]*School of Chemistry and Chemical Engineering, Jiangsu University, Zhenjiang, 212013, P. R. China.*
[b]*State Key Laboratory of Silicon Materials, Department of Materials Science and Engineering, Zhejiang University, Hangzhou, 310027, P. R. China.*
E-mail: liuyu@ujs.edu.cn

2. Experimental

2.1. Synthesis of Fe_3O_4 nanoparticles and graphene oxide (GO)

Fe_3O_4 nanoparticles were synthesized by the method reported previously.[23] 0.59 g of $FeCl_3 \cdot 6H_2O$ was dissolved in 40 mL of deionized water and heated up to 60 °C. After that, 0.14 g of $FeCl_2$ was added to the mixture followed by further stirring. Then quickly adding 1 mL of 28% ammonia solution, the mixture was allowed to react at 80 °C for 1 h. The whole reaction is described in Equation:

$$Fe^{2+}+2Fe^{3+}+8OH^- \rightarrow Fe_3O_4+4H_2O \quad (1)$$

The nanoparticles were isolated with the help of a magnet and washed 5 times, and then dispersed in 80 mL of water by ultrasonification. 0.31 g of p-sulfobenzoic acid potassium salt was dissolved in above dispersion with the assistance of sonication for 10 min. The resulted Fe_3O_4 nanoparticles were negatively charged with zeta potential of -24.4 mV and captured by magnet and washed with adequate water, finally dispersed in 500 mL of water for the preparation of composite films. The concentration of Fe_3O_4 suspension was 0.8 mg mL^{-1}. GO was prepared from graphite powder by a modified Hummers' method as described in our previous work[3] and the concentration of GO dispersion was 0.2 mg mL^{-1} with zeta potential of -47.0 mV.

2.2. Synthesis of Fe_3O_4/graphene films

A certain amount of Fe_3O_4 nanoparticle suspension and 10 mL GO dispersion were mixed together. Since the hydrogen bonding or intermolecular force between them, they quickly assembled with each other and formed flocculent precipitate within a few minutes. Subsequently, Fe_3O_4/GO lamellar films were prepared by filtering the mixed suspension on a polycarbonate membrane with 200 nm pores. The preparation route is demonstrated in Scheme 1. Three samples with mass ratios of Fe_3O_4 to GO of 1:1 (4 mg), 2:1 (6 mg), 1:2 (3 mg), were synthesized for comparison. Thermal reduction of Fe_3O_4/GO to Fe_3O_4/graphene was accomplished in a flow of N_2 at 600 °C for 2 h.

2.3. Electrode preparation

Fe_3O_4/graphene hybrid lamellar film was directly used as electrode, and incorporated into a coin-type cell with lithium foils as both counter and reference. The Fe_3O_4 electrode was prepared by mixing the active materials, carbon black, and polyvinylidenefluoride with a mass ratio of 8:1:1, and pasting onto pure copper foils, then pressed and dried under vacuum at 60°C for 12 h. The mass of Fe_3O_4/graphene (1:1), Fe_3O_4/graphene (2:1), Fe_3O_4/graphene (1:2) and pure Fe_3O_4 in the cycling performance tests are 0.9 mg, 1.3 mg, 0.8 mg and 1.1 mg, respectively. The mass of Fe_3O_4/graphene (1:1) in the rate test is 1.0 mg. The electrolyte employed in the cell was 1M LiPF6 in a 50:50 (w/w) mixture of ethylene carbonate and diethyl carbonate. The galvanostatic (GV) charge-discharge performances of the cell were tested in the voltage range of 0.01-3.0 V under a constant current density of 0.5 C by EQ-BST8-WA battery-test system, cyclic voltammetry (CV) was recorded by a CHI 660D electrochemical workstation in the voltage range 0.01-3.0 V with a scan rate of 0.1 mV s^{-1}. Electrochemical impedance spectroscopy (EIS) results were obtained from a frequency range of 100 kHz to 1 Hz.

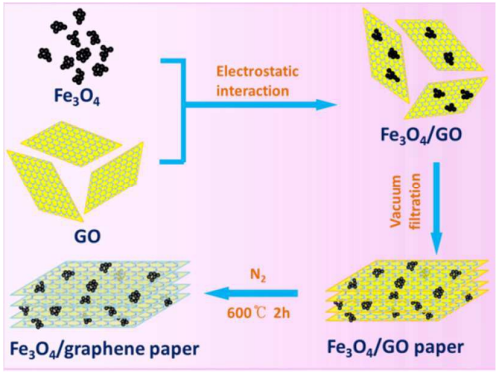

Scheme 1. Schematic illustration of the preparation process of the Fe_3O_4/graphene hybrid sandwiched films.

2.4. Characterization

The crystallinity of the composite was obtained by X-ray diffraction (XRD) at room temperature using an X'Pert PRO (PANalytical, Netherlands) instrument with Cu *Kα* radiation. The morphologies were characterized using scanning electronic microscopy (SEM) (Hitachi S-4800) and transmission electron microscopy (TEM, Philips CM200). Raman spectra were conducted on the Renishaw inVia Raman microscope under the excitation length of 532 nm. The specific surface area was calculated by Quantachrome Autosorb-1 apparatus

3. Results and discussion

3.1 Morphology and structures

Fig. 1 is the XRD patterns of Fe_3O_4/GO and Fe_3O_4/graphene composite films. For Fe_3O_4/GO composites, the weak diffraction peaks at 2θ values of 29.9°, 35.3°, 42.9°, 56.7° and 62.2° are observed, which match well with face-centered cubic Fe_3O_4 (JCPDS standard card no. 86-1354). Besides, a sharp diffraction peak emerges at ca. 9.4◦ also can be observed, which is corresponding to GO.[3] After thermal annealing treatment, the (001) diffraction peak at 24.2° is observed. This is due to the removing of interlayed water and oxygen functional groups.[7] Moreover, the Fe_3O_4 show sharper and stronger peaks than the original Fe_3O_4, suggesting that the high-temperature calcination improved the crystallinity of Fe_3O_4 nanoparticles and the particles grow bigger.

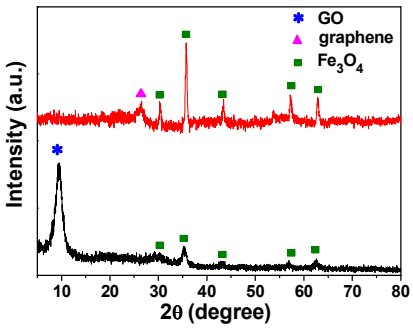

Fig. 1 XRD pattern of Fe_3O_4/GO and Fe_3O_4/graphene films

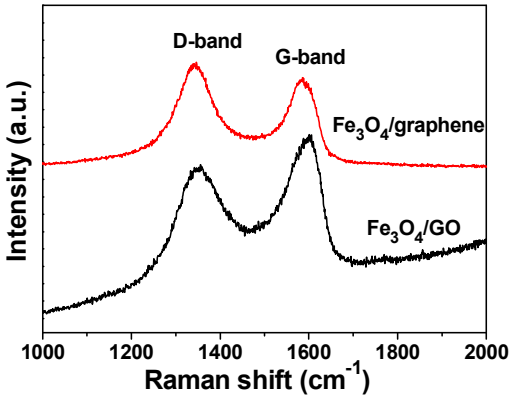

Fig. 2 Raman spectra of Fe_3O_4/GO and Fe_3O_4/graphene film

Raman spectroscopy is a versatile characterization tool to study the structural changes of graphene layers. Fig. 2 shows the Raman spectra of Fe_3O_4/GO and Fe_3O_4/graphene composites. Two characteristic peaks (D-bands and G-bands) of carbon based materials are observed. The intensity ratio of two bands (I_D/I_G) reflects the graphitization degree of carbon solids and density of defects in graphene-based materials.[24,25] Obviously, the Fe_3O_4/graphene shows an increased I_D/I_G value compared to the Fe_3O_4/GO, this indicates more defects were introduced into the Fe_3O_4/graphene under the thermal reduction of exfoliated GO.

Fig.3 shows the cross-section SEM images of Fe_3O_4/graphene hybrids films with different mass ratio of Fe_3O_4 to graphene. Upon incorporation of Fe_3O_4 nanoparticles into the highly lamellar graphene nanosheets, the Fe_3O_4 are uniformly intercalated between the graphene nanosheets and form porous network structures. The surface area of the composites is 68.3 m^2 g^{-1}, much higher than the pure graphene (14.9 m^2 g^{-1}) as reported before.[24] The Fe_3O_4 nanoparticles in the hybrid films expand the interlayer space between the graphene nanosheets and offer more opportunities for the electrolyte ions to access to the surface of electrochemical active materials. These homogenous porous structures are promising for the electrochemical applications. By increasing the amount of Fe_3O_4, more Fe_3O_4 are observed from the SEM images (Fig. 3a-c), which are consistent with the mass ratios of Fe_3O_4 to graphene. Especially in Fig.3a and b, the good connection between Fe_3O_4 and graphene can be clearly observed.

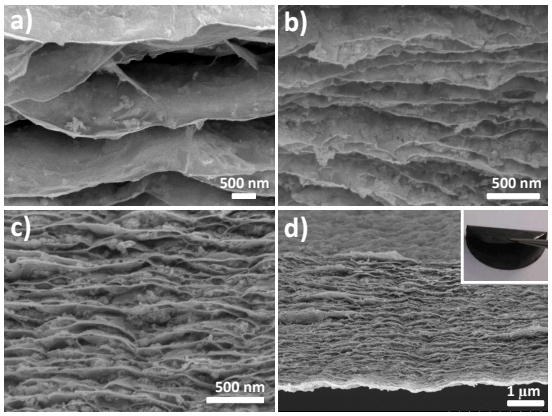

Fig. 3 The cross-section SEM images of Fe_3O_4/graphene hybrids films with different mass ratio of Fe_3O_4 to graphene of (a) 1:2, (b) 1:1 and (c, d) 2:1. Inset in (d) is a digital photograph of Fe_3O_4/graphene paper shows good flexibility

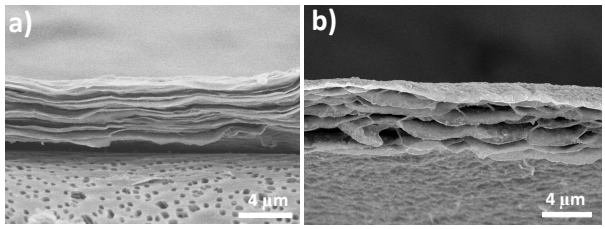

Fig. 4 Cross-section SEM images of stacking graphene film and Fe_3O_4/graphene composite film.

The unique structure is different from the most reports of simple stack, the good connection between Fe_3O_4 and graphene derived from hydrogen bonding or intermolecular force making them beneficial to charge transfer. As can be seen from Fig. 3d, the thickness of the composite film is about 6 μm. The inset in Fig. 3d shows that the Fe_3O_4/graphene paper with good flexibility can be used as binder free anodes and has potential in wearable devices.

Fig. 4 compares the cross-section SEM images of stacking graphene film and Fe_3O_4/graphene composite film. It is clearly seen that the graphene layers are tightly packed, which not good for electrolyte diffusion and applicable for Li storage. For Fe_3O_4/graphene composite film, the graphene nanosheets show an orderly and spaced structure. The porous composite films are favorable for the access of electrolyte and rapid diffusion of electrolyte ions, which is difficult to achieve in closely packed graphene paper. Besides, our self-assembling method is also different from those directive vacuum filtration method. The Fe_3O_4 nanoparticles assembled with the negatively charged GO, the surface functional groups of GO have changed a lot, thus, Van der Wals forces between them are also decreased, resulting in loose and porous structure.

Fig. 5a and b are the top-view SEM and TEM images of Fe_3O_4/graphene (1:1), it is clearly shown that Fe_3O_4 nanoparticles are anchored on the surface of graphene, which is consisted with the SEM results.

3.2 Electrochemical performances

Cyclic voltammograms was applied to investigate the electrochemical details of Fe_3O_4/graphene (1:1). The assembled cell was tested at a scan rate of 0.1 mV/s within the voltage window of 0.01-3.00 V (vs. Li/Li^+). As shown in Fig. 6a, in the first cathodic scan, the well-defined reduction peaks at 0.47 and 0.83 V correspond to formation of solid electrolyte interphase (SEI) layer generating on the electrode surface and Li_2O, the cathodic peak centered at 1.35 V corresponds to the structure transition caused by lithium insertion into Fe_3O_4 ($Fe_3O_4+xLi^++xe^-\rightarrow Li_xFe_3O_4$), which are not observed in the subsequent cycles. In subsequent cycles (2^{nd}, 3^{rd} and 4^{th}), the

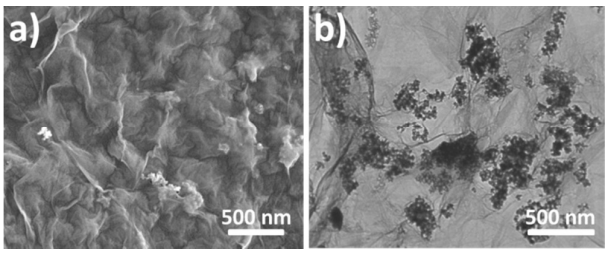

Fig. 5 SEM (a) and TEM (b) images of Fe_3O_4/grapheme

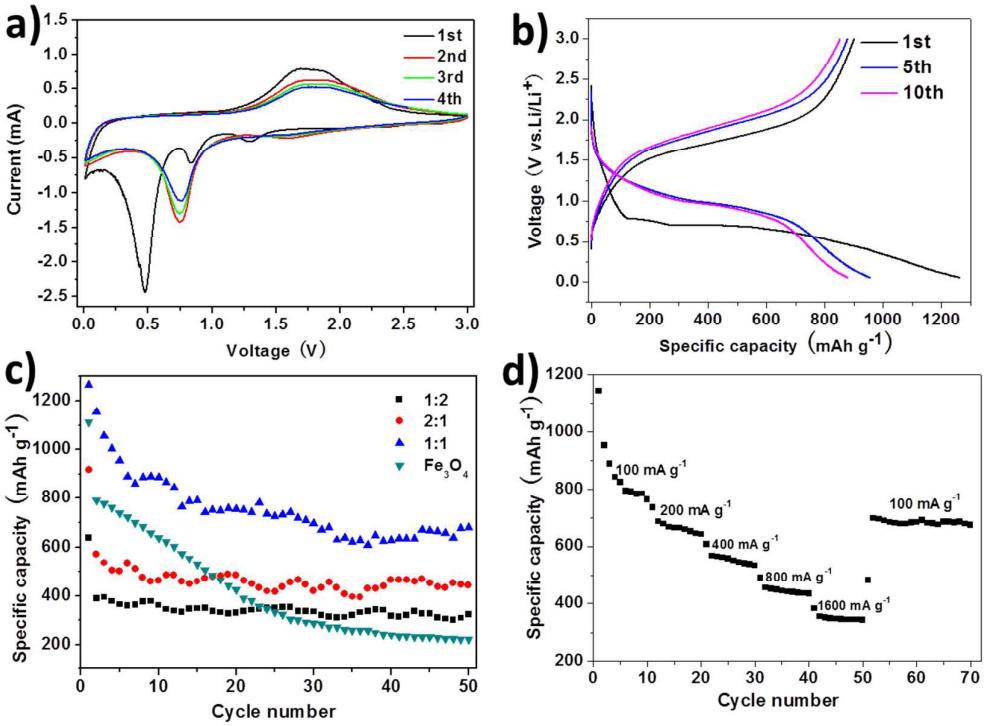

Fig. 6 (a) CV curves of Fe_3O_4/graphene (1:1) at a scan rate of 0.1 mV s^{-1}. (b) Charge-discharge curves of the Fe_3O_4/graphene (1:1). (c) Cycling performance of Fe_3O_4 and Fe_3O_4/graphene composites at 100 mA g^{-1}. (d) Cycling performance of Fe_3O_4/graphene (1:1) at different rates

reduction peak shifts to 0.75 V and tends to be stable, indicating that the redox reaction is well reversible. In the anodic scans, two weak peaks at 1.68 and 1.89 V are ascribing to the reversible electrochemical reduction/oxidation ($Fe_3O_4 \leftrightarrow Fe$) reactions.[13-18]

Fig. 6b presents the charge/discharge profiles of Fe_3O_4/graphene (1:1) in the 1st, 5th and 10th cycles at a current density of 100 mA g^{-1}. It can be seen a long potential plateau at approximately 0.7 V, this is a typically characteristic of the Fe_3O_4 electrodes during the first discharge process.[26,27] The first discharge and charge capacity is 1263.2 and 900.5 mA h g^{-1}, the irreversible capacity loss may be caused by the irreversible capacity loss, including inevitable formation of SEI and decomposition of electrolyte, which are common to most anode materials.[28,29]

Fig. 6c compares the cycling performance of pure Fe_3O_4 and Fe_3O_4/graphene composites with different mass ratios of Fe_3O_4 to graphene. The capacity fade of pure Fe_3O_4 is rather severe and after 50 cycles is reduced to only 222.0 mA h g^{-1}, while the capacity fade of Fe_3O_4/graphene substantially less than that of pure Fe_3O_4, for Fe_3O_4/graphene (1:2), Fe_3O_4/graphene (2:1) and Fe_3O_4/graphene (1:1), the capacity still remained 324.1, 442.6 and 681.2 mA h g^{-1}. It is well known that the capacity loss in Fe_3O_4 is mainly caused by the volume changes in lithium ion intercalation and deintercalation processes and the poor electron conductivity. The incorporation of graphene not only increased the conductivity of Fe_3O_4, but also kept the Fe_3O_4 nanoparticles in good electronic contact to accommodate the volume changes.

Rate performance is an important precondition to apply as anode material in high power LIBs. Therefore, Fig. 6d shows the rate performance of the as-prepared Fe_3O_4/graphene (1:1) at different current densities. The discharge capacities of the Fe_3O_4/graphene (1:1) at 100, 200, 400, 800, and 1600 mA g^{-1} are, 763.3, 642.5, 533.6, 434.2, and 342.9 mA h g^{-1}, respectively, demonstrating an excellent high rate performance. It is worth noting that as long as the current rate reverses back to 100 mA g^{-1}, the cell capacity recovers to the original value, indicating that the Fe_3O_4/graphene composite is tolerant of various charge and discharge currents. In our case, the porous structure can provide 3D electron conducting channels within the electrode, and facilitate the penetration and diffusion of electrolyte, leading to fast lithium ion transport.

In order to deeply understand the electrochemical performance of the Fe_3O_4 nanoparticles and Fe_3O_4/graphene film, we further compares the Nyquist plots of the two samples after 50 cycles. As

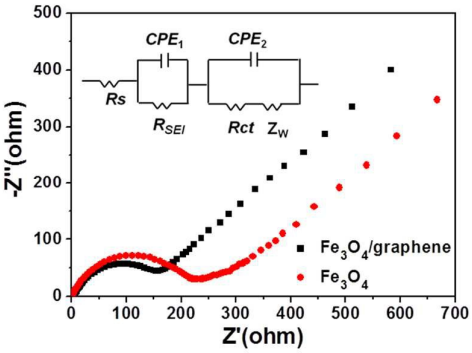

Fig. 7 Nyquist plots of impedance for Fe_3O_4 and Fe_3O_4/graphene hybrids films after 50 cycles. (All measurements were conducted in the delithiated state)

Table 1. Impedance parameters derived using an equivalent circuit model for Fe_3O_4 nanoparticles Fe_3O_4/graphene hybrids films electrodes after 50 cycles

electrode	R_s (Ω)	R_{SEI} (Ω)	R_{ct} (Ω)	Z_W (Ω $s^{-1/2}$)
Fe_3O_4 (50^{th})	3.2	84.5	154.7	78.5
Fe_3O_4/graphene(50^{th})	21	43.6	115.8	42.6

shown in Fig. 7, the spectra appeared in the medium frequency range is classically assigned to the charge-transfer resistance occurring between active materials and liquid electrolyte. The approximately 45° inclined line in the low frequency range corresponds to the Warburg impedance (Z_w) is related to the diffusion of Li ions into the bulk of the active materials.[3,15] The inset in Fig. 7 is an equivalent circuit model of the studied system. R_s and R_{ct} are the ohmic resistance (total resistance of the electrolyte, separator, and electrical contacts) and charge-transfer resistance, respectively. R_{SEI} is the impedance related with to the SEI film. CPE is the constant phase-angle element, involving double layer capacitance. The fitted impedance parameters can be found in Table 1. Apparently, the Fe_3O_4/graphene anode shows a relatively lower charge transfer resistance of 115.8 Ω than 154.7 Ω of the pure Fe_3O_4 anode. This implies that the graphene make charge transfer much easily at the electrode/electrolyte interface, and consequently decrease the internal resistance for both electrons and lithium ions. Furthermore, Z_W of Fe_3O_4/graphene is lower than Fe_3O_4, which confirms that the interbedded Fe_3O_4 enable good electrolyte penetration between graphene nanosheets.

We further observed the cross-section SEM image (Fig. 8) of the Fe_3O_4/graphene paper after 50 cycles. The activity material still maintains its original structure. The graphene layers without major structural damage can be seen clearly, but the Fe_3O_4 nanoparticles are relatively agglomerated. As a result, the integrity of graphene nanosheets in the anode is responsible for the enhanced cycling stability compared to pure Fe_3O_4 nanoparticles for lithium storage in long-term cycling.

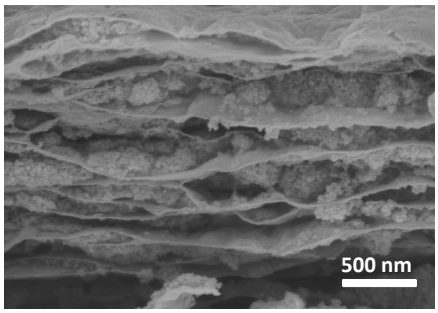

Fig. 8 SEM image of Fe_3O_4/graphene hybrids films after 50 cycles

4. Conclusions

We have successfully synthesized Fe_3O_4 nanoparticles anchored graphene nanosheets. The sandwiched structure can offer efficient electrically conducting channels for fast lithium ion diffusion and buffer the severe volume changes associated with lithium insertion/extraction process. Therefore, as flexible and binder-free Li-ion batteries anode, this unique structure demonstrates high reversible capacity of 681.2 mA h g^{-1} after 50 cycles and excellent cycling stability as well as superior rate capacities. The composite film has the potential for flexible electrochemical energy storage devices.

Acknowledgements

This work was supported by Start-Up Foundation of Jiangsu University (15JDG144), the National Natural Science Foundations of China (NSFC 21271154, 51272232), the national basic research program of china 973 program (2015CB655302), and Natural Science Foundation for Outstanding Young Scientist of Zhejiang Province, China (LR14E020001).

References

1 D. N. Wang, J. L. Yang, X. F. Li, D. S. Geng, R.Y. Li, M. Cai, T. K. Sham and X. L. Sun, *Energy. Environ. Sci*., 2013, **6**, 2900-2906.

2 M. Zhang, X. H. Hou, J. Wang, M. Li, S. j.J Hu, Z. P. Shao and X. Liu, *J. Alloys Compd*., 2014, **588**, 206-211.

3 Y. Liu, W. Wang, L. Gu, Y. W. Wang, Y. L. Ying, Y. Y. Mao, L. W. Sun and X. S. Peng, *ACS Appl. Mater. Interfaces*, 2013, **5**, 9850-9855.

4 G. L. Wu, M. B. Wu, D. Wang, L. H. Yin, J. S. Ye, S. Z. Deng, Z. Y. Zhu, W. J. Ye and Z. T. Li, *Appl. Surf. Sci*.,2014, **315**, 400-406.

5 T. Hu, X. Sun, H. T. Sun, M. P. Yu, F. Y. Lu, C. S. Liu and J. Lian, *Carbon*, 2013, **51**, 322-326.

6 R. Liu, T. Li, F. D. Han, Y. J. Bai, Y. X. Qi and N. Lun, *J. Alloys Compd*., 2014, **597**, 30-35.

7 B. Jin, A. H. Liu, G. Y. Liu, Z. Z. Yang, X. B. Zhong, X. Z. Ma, M. Yang and H. Y. Wang, *Electrochim. Acta*, 2013, **90**, 426-432.

8 N. Q. Zhao, S. Wu, C. N. He, Z. Y. Wang, C. S. Shi, E. Z. Liu and J. J. Li, *Carbon*, 2013, **57**, 130-138.

9 C. Lei, F. Han, Q. Sun, W. C. Li and A. H. Lu, *Chem. Eur. J*.,2014, **20**, 139-145.

10 J. Luo, J. Liu, Z. Zeng, C. F. Ng, L. Ma, H. Zhang, J. Lin, Z. Shen and H. J. Fan, capability, *Nano Lett*., 2013, **13**, 6136-6143.

11 B. Y. Jung, H. S. Lim, Y. K. Sun and K.D. Suh, *J. Power Sources*, 2013, **244**, 177-182.

12 J. Zang, J. J. Chen, C. L. Zhang, H. Qian, M. S. Zheng, and Q. F. Dong, *J. Mater. Chem. A*, 2014, **2**, 6343-6347.

13 Y. R. Wang, L. Zhang, X. H. Gao, L. Y. Mao, Y. Hu and X. W. (David) Lou, *Small*, 2014, **10**, 2815-2819.

14 J. Z. Liu, J. F. Ni, Y. Zhao, H. B. Wang and L. J. Gao, *J. Mater. Chem. A*, 2013, **1**, 12879-12884

15 R. H. Wang, C. H. Xu, J. Sun, L. Gao and C. C. Lin, *J. Mater. Chem. A*, 2013, **1**, 1794-1800.

16 Y. Chen, B. H. Song, X. S. Tang, L. Lu, J. M. Xue, *J. Mater. Chem*., 2012, **22**, 17656-17662.

17 Q. Zhou, Z. B. Zhao, Z. Y. Wang, Y. F. Dong, X. Z. Wang, Y. Gogotsi and J. S. Qiu, *Nanoscale*, 2014, **6**, 2286-2291.

18 K. Zhang, W. Zhao, J. T. Lee, G. Jang, X. J. Shi and J. H. Park, *J Mater. Chem. A,* 2014, **2**, 9636-9644.

19 H. Gwon, J. Hong, H. Kim, D. H. Seo, S. Jeon and K. Kang, *Energy Environ. Sci*., 2014, **7**, 538-551.

20 J. A. Rogers, T. Someya and Y. G. Huang, *Science*, 2010, **327**, 1603-1607.

21 Y. Qian, A. Vu, W. Smyrl and A. Stein, *J. Electrochem. Soc.*, 2012, **159**, 1135-1140.

22 L. Noerochim, J. Z. Wang , D. Wexler, Z. Chao and H. K. Liu, J. *Power Sources*, 2013, **228**, 198-205.

23 X. S. Peng, J. Jin, E. M. Ericsson and I. Ichinose, *J. Am. Chem. Soc.*, 2007, **129**, 8625-8633.

24 Y. Liu, Y. L. Ying, Y. Y. Mao, L. Gu, Y. W. Wang and X. S. Peng, *Nanoscale*, 2013, **5**, 9134-9140.

25 J. F. Liang, Y. Zhao, L. Guo and L. D. Li, *ACS Appl. Mater. Interfaces*, 2012, **4**, 5742-5748.

26 S. Bhuvaneswari, P. M. Pratheeksha, S. Anandan, D. Rangappa, R. Gopalanb and T. N. Rao, *Phys. Chem. Chem. Phys*., 2014, **16**, 5284-5294.

27 J. L. Liu, H.B. Feng, X. P. Wang, D. Qian, J. B. Jiang, J. H. Li, S. J. Peng, M. Deng and Y. C. Liu, *Nanotechnology*, 2014, **25**, 225401.

28 D. L. Ma, S. Yuan and Z. Y. Cao, *Chin. Sci. Bull*, 2014, **59**, 2017-2023.

29 Y.P. Liu, K. Huang, H. Luo, H. X. Li, X. Qi and J. X. Zhong, *RSC Adv*., 2014, **4**, 17653-17659.

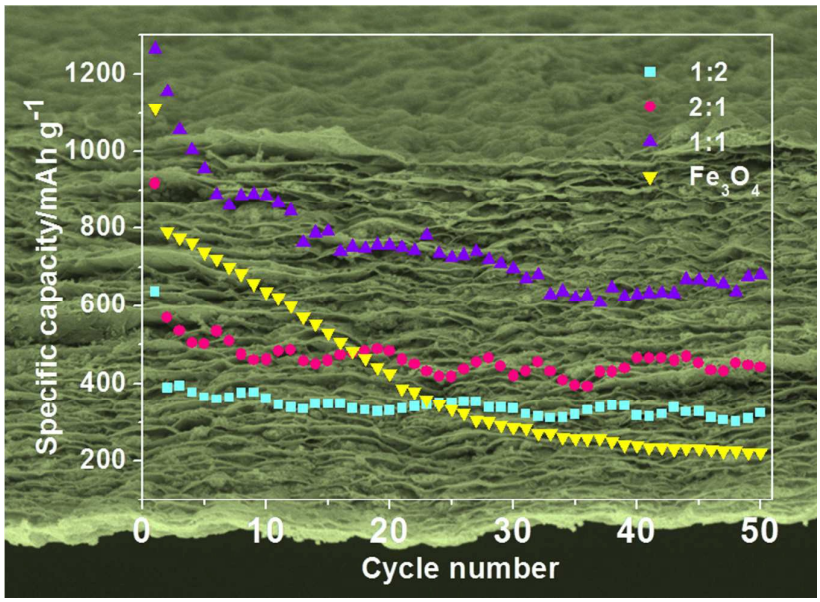

Fe_3O_4 nanoparticles homogeneously decorated onto layered graphene nanosheets film exhibits excellent cyclic retention and good rate capability when used as anode in lithium storage.